Delay-dependent Wide-area Damping Controller Synthesis Approach Using Jensen's Inequality and Evolution Algorithm

Wencheng Wu, *Member*, *IEEE*, *Senior Member CSEE*, Xiaoru Wang, *Senior Member*, *IEEE*, Hong Rao, *Fellow IEEE*, *Fellow CSEE*, and Baorong Zhou

***Abstract*—A time-delay-dependent wide-area damping controller synthesis approach, based on Jensen's integral inequality and evolution algorithm, is developed to suppress the adverse effect of time delay on the supplemental control of high-voltage direct current (DC) transmission systems. Initially, the state-space model of hybrid AC/DC systems with time delay is derived and the delay-dependent criteria for the stability of the closed-loop system are provided based on Jensen's integral inequality. Subsequently, initial solutions are randomly generated to overcome the difficulty of solving the nonlinear matrix inequality. Finally, the time-delay stability upper bound of the controller is optimized using the differential evolution algorithm. In comparison to popular time-delay stable controller design methods, such as the free-weighting-matrix approach, the proposed method based on output feedback realization requires fewer decision variables and is more suitable for large-scale hybrid AC/DC systems. Three examples are introduced to verify the effectiveness of the proposed method.**

***Index Terms*—Damping suppression, delay-dependent control, differential evolution algorithm, Jensen's inequality, output feedback, time-varying delay, wide-area control.**

I. Introduction

LOW-FREQUENCY oscillations pose a serious threat to the security and stability of large-scale interconnected power systems. The use of supplemental control functions of high-voltage direct current (HVDC) or wide-area power system stabilizers allows the control of the cross-area oscillation patterns and is one of the most widely studied measures. However, in practical applications, wide-area control systems, such as multi-DC coordinated control systems, must collect multiple signals which are thousands of kilometers apart. Thus, the impact of signal transmission delays on the control effect cannot be ignored.

Manuscript received May 23, 2021; revised August 5, 2021; accepted September 7, 2021. Date of online publication May 6, 2022; date of current version September 22, 2022. This work was supported by the National Key Research and Development Program of China (2016YFB0901001).

W. C. Wu (corresponding author, e-mail: Wencheng_Wu@my.swjtu.edu.cn) and X. R. Wang are with the School of Electrical Engineering, Southwest Jiaotong University, Chengdu, Sichuan Province 610021, China. W. C. Wu is also with the Southwest Electric Power Design Institute, Sichuan Province 610056, China.

H. Rao and B. R. Zhou are with the State Key Laboratory of HVDC, Electric Power Research Institute, CSG, Guangzhou 510663, China.

DOI: 10.17775/CSEEJPES.2021.03990

Wide-area measurement and control signals in power systems can be transmitted in several ways, e.g., through optical fibers, carrier waves, and satellites. According to [1], [2], optical fiber transmission has the shortest time delay, generally in the range of 60 to 100 ms, while the time delay of satellite transmission can be up to 560 ms [3].

Based on current research [4]–[7], considering the time consumption of signal collection, calculation, and transmission, the maximum signal delays of measurement-type and protection-type PMUs are found to be more than 600 ms and 40 ms, respectively. Therefore, the design of wide-area controllers without considering the time delay may lead to system instability [5]–[7]. Thus, the fixed delay compensation algorithm is generally implemented in wide-area control projects; however, it is observed that the expected effect is not achieved with actual applications. Regarding controller performance degradation, owing to inaccurate delay compensation, parts of the wide-area control systems are only employed as low-frequency oscillation monitoring and warning systems, without being used for closed-loop operations [8], thereby losing their utility. To improve the performance of wide-area control systems, methods for time-delay stability analysis, time-delay limit estimation, and time-delay system stabilization are required.

Current methods are divided into frequency- and time-domain methods. The theoretical basis of the frequency-domain method is a sufficient and necessary condition for the stability of a linear system. The roots of the characteristic equations are located in the left half of the complex plane. However, the system equation obtained by Laplace transformation is a transcendental equation that is difficult to solve, especially when the time delay varies with time or when uncertainties exist in the system. Current research on frequency-domain methods focuses on analyzing and synthesizing fixed time-delay systems; among these, the most successful methods are the DDE-BIFTool [9] and spectral method [10], which can handle large-scale systems. The frequency-domain synthesis methods include the lead-lag compensation method, linearization method based on the Pade equation, Dahlin algorithm for PID, Smith algorithm [11], and spectral method [12]. These methods can only handle fixed time delays with low accuracy and, thus, their practical application is significantly limited.

In contrast, time-domain methods are based on the stability theorems of Lyapunov–Krasovskii (L–K) and Rzumishin,

2096-0042 © 2021 CSEE. This is an open access article under the CC BY-NC-ND license (http://creativecommons.org/licenses/by-nc-nd/4.0/).

which involve constructing the appropriate Lyapunov or L–K functional for delay-dependent stability and applying the linear matrix inequality (LMI) technique. The widely used methods in this field are the model transformation methods and free-weighting-matrix methods. Existing model transformation methods primarily focus on the bounding of the cross terms that appear in the L–K functional derivatives and applying Park's inequality and Moon's inequality to estimate the bounds of the cross terms to reduce the conservativeness of the methods. The weight matrices introduced by the model transformation method are fixed, leading to its greater conservativeness. The free-weighting-matrix (FWM) method addresses this issue by replacing the weight matrices containing state variables, such as, $x(t)$, $\dot{x}(t)$ and $x(t-d)$, in the L–K functional with free-weight matrices composed of adjustable elements. Introducing a higher number of free-weight matrices improves the estimation accuracy of the time-delay upper bound. The FWM method and its improved variations have obtained the best results reported thus far. Through the cone complement linearization (CCL) algorithm, the FWM method can be used for controller synthesis, as well as controller performance analysis [13], [14]. The FWM method has also been widely applied for the wide-area control of power systems. For example, Ma *et al*. [15] used the FWM method for the delay-stability performance analysis of an HVDC supplemental controller. Li *et al*. [16] and Yong *et al*. [17] applied the FWM method to design a time-delay state feedback controller for HVDC supplemental control and wide-area control.

However, although the introduction of FWMs greatly reduces the conservativeness of the delay-stability analysis, it also greatly increases the scale of the system LMIs, making it particularly difficult to generalize the method to large-scale systems. Its controller design method, based on the CCL algorithm, is a local optimization method with conservative effects. To reduce the conservativeness of the delay-stability criteria and the number of decision variables, criteria based on Jensen's inequality and Wirtinger's inequality have been widely studied. Jensen's inequality has attracted considerable attention owing to its low conservativeness and low number of decision variables required. Jensen's integral inequality was extended to time-delay systems [18], [19] and has been applied to construct the time-delay stability criteria based on the L–K functional [20]–[23]. According to the above reports, Jensen's method can account for the interval delay and time-varying delay with few decision variables and obtain less conservative results. It can achieve a calculation accuracy comparable to that of the FWM method, with a much higher computational efficiency.

The state-space equations of power systems are large-scale. A simple 4-machine 2-zone system model has nearly 100 state equations. According to our statistics, the current computational data of the Chinese interconnected power system consists of up to 80,000 nodes and the order of the state equation is approximately 50,000. Although the controller can be designed on a reduced-order system using the model reduction method, it is still difficult to apply the FWM method for analysis, even for small-scale power systems, owing to the large number of additional variables introduced. Moreover, it is found that applying the FWM method to systems that exceed 40 orders is impossible. The required decision variables based on Jensen's inequality are significantly reduced while retaining relatively high accuracy; however, when conducting output-feedback controller design, the matrix inequality to be solved involves the product term of two unknown matrices because the controller parameters are unknown; thus, bilinear matrix inequality is introduced, which is an NP-hard problem. Therefore, time-delay control synthesis based on Jensen's inequality method is very difficult compared to the FWM method, which can apply the very effective CCL algorithm. Thus far, controller synthesis methods, based on Jensen's inequality, have not been proposed.

The static output feedback (SOF) or dynamic output feedback (DOF) controller synthesis process introduces bilinear matrix inequalities; solving these is an NP-hard problem, which is challenging to address. However, if the controller is obtained by a randomly generated method, the problem can be transformed into the LMI form. The time-delay stability of the closed-loop system can be checked using the LMI techniques. The maximum allowable delay bound (MADB) can be determined by increasing the time-delay upper bound until the closed-loop system loses its stability. This is the current foundation of applying stochastic methods to design SOF/DOF controllers [24], [25], but it is less efficient as there is no optimization process, which is a typical "generation-check" idea of the stochastic method. Given the efficiency of the differential evolution (DE) algorithm in solving nonlinear and nonconvex problems, it is expected that the efficiency of the design method can be increased by introducing the DE algorithm to provide the optimized search direction, and better controller parameters can be obtained.

In this study, the Jensen's inequality method is extended to design a time-delay controller for the wide-area control system, and a DE-LMI hybrid algorithm is applied to acquire the SOF/DOF controller parameters, so as to reduce the conservativeness and improve the computational efficiency.

The remainder of this paper is organized as follows. Section II presents the theoretical basis of Jensen's inequality time-delay stability analysis method. Section III presents the establishment of the output-feedback controller design method by using the Jensen's inequality and DE algorithm. The algorithm flow for the proposed method is illustrated in Section IV. The validity of the proposed method is verified by three numerical simulation examples presented in a case study in Section V. The conclusion is presented in Section VI.

II. Theoretical Basis

A. Problem Description

The state equation of a hybrid AC/DC system considering the signal transmission delay can be expressed as follows:

$$\begin{cases} \dot{\boldsymbol{x}}(t) = \boldsymbol{A}\boldsymbol{x}(t) + \boldsymbol{B}\boldsymbol{u}(t) \\ \boldsymbol{y}(t) = C\boldsymbol{x}(t - \mathrm{d}(t)) \\ \boldsymbol{x}(t) = \boldsymbol{\varphi}(t), -h \le t \le 0 \end{cases} \tag{1}$$

where $\boldsymbol{x}(t) \in R^n$ is the state variable, n is a positive integer, $\boldsymbol{A}$, $\boldsymbol{B}$, and $\boldsymbol{C}$ are constant matrices of suitable dimensions, h is

the upper bound of the time delay, and $\mathrm{d}(t)$ is a delay-varying function.

The following dynamic output-feedback control law is applied to (1):

$$\boldsymbol{K}_s : \begin{cases} \dot{\boldsymbol{\eta}}(t) = \boldsymbol{A}_k \boldsymbol{\eta}(t) + \boldsymbol{B}_k \boldsymbol{y}(t) \\ \boldsymbol{u}(t) = \boldsymbol{C}_k \boldsymbol{\eta}(t) + \boldsymbol{D}_k \boldsymbol{y}(t) \end{cases} \tag{2}$$

where $\boldsymbol{A}_k \in \boldsymbol{R}^{n_k \times n_k}$, $\boldsymbol{B}_k \in \boldsymbol{R}^{n_k \times n_y}$, $\boldsymbol{C}_k \in \boldsymbol{R}^{n_u \times n_k}$, and $\boldsymbol{D}_k \in \boldsymbol{R}^{n_u \times n_y}$. Here, K_s can be chosen as a reduced-order controller $(n_k < n_x)$ or a full-order controller $(n_k \geq n_x)$.

If $\boldsymbol{x}_\mathrm{c} = \begin{bmatrix} \boldsymbol{x} \\ \boldsymbol{\eta} \end{bmatrix}$, the closed-loop system can be written as follows:

$$\dot{\boldsymbol{x}}_\mathrm{c}(t) = \boldsymbol{A}_\mathrm{c} \boldsymbol{x}_\mathrm{c}(t) + \boldsymbol{A}_\mathrm{dc} \boldsymbol{x}_\mathrm{c}(t-h) \tag{3}$$

where

$$\begin{aligned} \boldsymbol{A}_\mathrm{c} &= \begin{bmatrix} \boldsymbol{A} & \boldsymbol{B}\boldsymbol{C}_k \\ \boldsymbol{0} & \boldsymbol{A}_k \end{bmatrix} = \overline{\boldsymbol{A}} + \overline{\boldsymbol{B}\boldsymbol{K}\boldsymbol{C}}, \\ \boldsymbol{A}_\mathrm{dc} &= \begin{bmatrix} \boldsymbol{B}\boldsymbol{D}_k\boldsymbol{C} & \boldsymbol{0} \\ \boldsymbol{B}_k\boldsymbol{C} & \boldsymbol{0} \end{bmatrix} = \overline{\boldsymbol{B}\boldsymbol{K}\boldsymbol{C}}, \end{aligned} \tag{4}$$

$$\begin{aligned} \overline{\boldsymbol{A}} &= \begin{bmatrix} \boldsymbol{A} & \boldsymbol{0} \\ \boldsymbol{0} & \boldsymbol{0} \end{bmatrix}, \quad \overline{\boldsymbol{B}} = \begin{bmatrix} \boldsymbol{B} & \boldsymbol{0} \\ \boldsymbol{0} & \boldsymbol{I} \end{bmatrix}, \\ \overline{\boldsymbol{C}} &= \begin{bmatrix} \boldsymbol{C} & \boldsymbol{0} \\ \boldsymbol{0} & \boldsymbol{I} \end{bmatrix}, \quad \boldsymbol{K} = \begin{bmatrix} \boldsymbol{D}_k & \boldsymbol{C}_k \\ \boldsymbol{B}_k & \boldsymbol{A}_k \end{bmatrix} \end{aligned} \tag{5}$$

B. Main Lemma

Consider the following time-delay state-space equations:

$$\dot{\boldsymbol{x}}(t) = \boldsymbol{A}\boldsymbol{x}(t) + \boldsymbol{A}_\mathrm{d}\boldsymbol{x}(t - \mathrm{d}(t)), \quad t > 0, \tag{6}$$

$$\boldsymbol{x}(t) = \boldsymbol{\phi}(t), \quad t \in [-h, 0], \tag{7}$$

$$0 < \mathrm{d}(t) < h, \quad \dot{\mathrm{d}}(t) \leq \mu. \tag{8}$$

where $\boldsymbol{A}_\mathrm{d}$ is a constant matrix of suitable dimensions and μ is a constant scalar that indicates the upper bound of the rate of change of the time delay.

Lemma 1 (Jensen's integral inequality)**.** for any symmetric positive definite matrix $\boldsymbol{M} \in \boldsymbol{R}^{n \times n}$, scalar r_1 and r_2 satisfying $r_1 < r_2$, vector function $\boldsymbol{\omega}[r_1, r_2] \to \boldsymbol{R}^n$, the following integral inequality holds:

$$\begin{aligned} &\left(\int_{r_1}^{r_2} \boldsymbol{\omega}(s)\mathrm{d}(s)\right)^\mathrm{T} \boldsymbol{M} \left(\int_{r_1}^{r_2} \boldsymbol{\omega}(s)\mathrm{d}(s)\right) \\ &\quad \leq (r_2 - r_1) \int_{r_1}^{r_2} \boldsymbol{\omega}^\mathrm{T}(s)\boldsymbol{M}\boldsymbol{\omega}(s)\mathrm{d}(s) \end{aligned} \tag{9}$$

Lemma 2 (time-delay stability criterion based on Jensen's integral inequality)**.** given scalars $h > 0$ and μ, if there exist symmetric matrices $\boldsymbol{P} = \boldsymbol{P}^\mathrm{T} > 0$, $\boldsymbol{Q} = \boldsymbol{Q}^\mathrm{T} \geq 0$, $\boldsymbol{S} = \boldsymbol{S}^\mathrm{T} > 0$, and $\boldsymbol{V} = \boldsymbol{V}^\mathrm{T} > 0$, such that the following LMI holds:

$$\boldsymbol{\Psi}_1 = \boldsymbol{\Psi} - [\boldsymbol{I} \quad -\boldsymbol{I} \quad \boldsymbol{0}]^\mathrm{T} \boldsymbol{V} [\boldsymbol{I} \quad -\boldsymbol{I} \quad \boldsymbol{0}] < \boldsymbol{0}, \tag{10}$$

$$\boldsymbol{\Psi}_2 = \boldsymbol{\Psi} - [\boldsymbol{0} \quad \boldsymbol{I} \quad -\boldsymbol{I}]^\mathrm{T} \boldsymbol{V} [\boldsymbol{0} \quad \boldsymbol{I} \quad -\boldsymbol{I}] < \boldsymbol{0} \tag{11}$$

where

$$\begin{aligned} \boldsymbol{\Psi} = &\begin{bmatrix} \boldsymbol{\Psi}_\mathrm{o} & \boldsymbol{P}\boldsymbol{A}_\mathrm{d} + \boldsymbol{V} & \boldsymbol{0} \\ * & -(1-u)\boldsymbol{Q} - 2\boldsymbol{V} & \boldsymbol{V} \\ * & * & -\boldsymbol{S} - \boldsymbol{V} \end{bmatrix} \\ &+ [\boldsymbol{A} \quad \boldsymbol{A}_d \quad \boldsymbol{0}]^\mathrm{T} \left(h^2\boldsymbol{V}\right) [\boldsymbol{A} \quad \boldsymbol{A}_\mathrm{d} \quad \boldsymbol{0}] \\ \boldsymbol{\Psi}_\mathrm{o} = &\boldsymbol{P}\boldsymbol{A} + \boldsymbol{A}^\mathrm{T}\boldsymbol{P} + \boldsymbol{Q} + \boldsymbol{S} - \boldsymbol{V} \end{aligned} \tag{12}$$

Then, the linear system with time-varying time delay described by (6)–(8) is asymptotically stable. The proof is provided in Appendix A.

III. Delay-dependent stability synthesis algorithm based on Jensen's integral inequality and DE-LMI algorithm

A. Research Approach

After obtaining $\boldsymbol{A}_\mathrm{c}$ and $\boldsymbol{A}_\mathrm{dc}$ of the closed-loop system, Lemma 2 still cannot be applied directly to obtain the output-feedback controller owing to the following three problems:

1) In closed-loop systems, (6) and (7) contain product terms, such as $\boldsymbol{P}\boldsymbol{A}_\mathrm{dc}$ and $h^2\boldsymbol{A}_\mathrm{c}\boldsymbol{R}\boldsymbol{A}_\mathrm{dc}$, which consist of two or three unknown matrices. They are nonlinear matrix inequalities that cannot be solved by linear matrix methods.

2) Lemma 2 can only judge whether a time-delay system is stable for a given time delay and its maximum rate of change; it cannot provide the MADB for a given feedback control law directly (the MADB is an important performance index to evaluate the effectiveness of controller synthesis methods).

3) The MADB of initially generated controllers does not necessarily meet the requirements and the above lemmas do not aid the optimization of the MADB.

To address these problems, this method first randomly generates a series of controllers $\boldsymbol{K}_s$, such that at most one unknown matrix will appear in (6) and (7), which can thus be solved by applying the LMI algorithm. The MADBs of the randomly generated controllers $\boldsymbol{K}_s$ can be determined by iteratively checking Lemma 2 using the bisection search method. To optimize the controller performance, the DE algorithm is applied to generate a new generation of controllers to be tested and the optimized controllers are obtained via iterative computations. Fig. 1 shows a flowchart of the time-delay-dependent stable synthesis algorithm applying Jensen's inequality and DE-LMI.

B. Random Generation Method for Controller

The controller matrix $\boldsymbol{K}_s$ is expressed as:

$$\boldsymbol{K}_{\boldsymbol{s}} = \begin{bmatrix} k_{11} & k_{12} & \cdots & k_{1(n_y+n_k)} \\ k_{21} & k_{22} & \cdots & k_{2n_y(n_y+n_k)} \\ \vdots & \vdots & \ddots & \vdots \\ k_{(n_\mathrm{u}+n_k)1} & k_{(n_\mathrm{u}+n_k)2} & \cdots & k_{(n_\mathrm{u}+n_k)(n_\mathrm{u}+n_k)} \end{bmatrix} \tag{13}$$

Because the DE algorithm can only optimize one-dimensional vectors, matrix $\boldsymbol{K}_{\boldsymbol{s}}$ is converted to the following one-dimensional row vector $\boldsymbol{K}$:

$$\begin{aligned} \boldsymbol{K} &= \begin{bmatrix} k_{11} & k_{12} & \ldots & k_{1(n_y+n_k)} & k_{21} & \ldots & k_{(n_u+n_k)(n_y+n_k)} \end{bmatrix} \\ &= \begin{bmatrix} k_1 & k_2 & \ldots & k_{n_y} & k_{n_y+n_k+1} & \ldots & k_{(n_u+n_k)(n_y+n_k)} \end{bmatrix} \end{aligned} \tag{14}$$

The above vector can be expressed as:

$$\boldsymbol{K} = \{(k_1, k_2, \ldots, k_{n_v}) \mid 1_i \leq k_i \leq u_i,$$

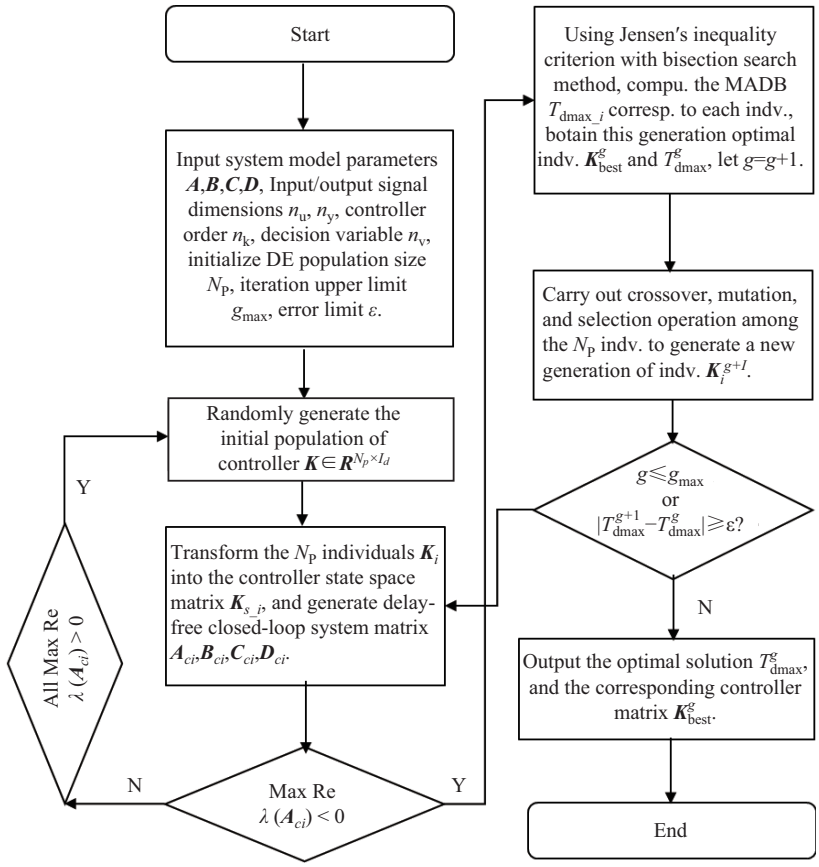

Fig. 1. Flow chart of proposed algorithm.

$$n_v = (n_{\mathrm{u}} + n_k) \times (n_{\mathrm{y}} + n_k)\} \tag{15}$$

Suppose that the value range of element k_i of vector $\boldsymbol{K}$ is $[k_{i\,\min}, k_{i\,\max}]$, and that an initial population of controllers with N_p individuals is randomly generated using the following rules:

$$\begin{cases} \boldsymbol{K}_{ij}^g = k_{\min} + \mathrm{rand}() \cdot (k_{\max} - k_{\min}) \\ i = 1, 2, \cdots, N_{\mathrm{P}}; \quad j = 1, 2, \cdots, n_v \end{cases} \tag{16}$$

where $\boldsymbol{K}_{ij}^g$ denotes the j-th dimensional component of the i-th individual of the controller in the g-th generation; N_{p} is the population size, which is the number of controllers to be tested in this generation; the $\mathrm{rand}()$ function produces a random number in the interval [0, 1], and K_i^g denotes the i-th individual of the controller in the g-th generation. The value range of the element k_i can be determined according to the prior knowledge of the controller. It can also be determined using a "trial and error" method, i.e., testing the following value ranges in turn: -10–10, -10^2–10^2, $\cdots$, -10^n–10^n. In most cases, only a few attempts are required to determine the correct value range.

C. Search Method for the Upper Bound of the Time-Delay Stability

After obtaining the controller with the random generation method, (6) and (7) still contain product terms, such as $h^2\boldsymbol{A}_{\mathrm{c}}\boldsymbol{R}\boldsymbol{A}_{\mathrm{dc}}$, which are still nonlinear matrix inequalities. However, because the unknown variable h is one-dimensional, the MADB can be obtained by the search method. To improve the efficiency of the search, the bisection search method is used as follows:

Step 1: Set the step size Δh, the maximum number of iterations *Iter_max*, and the error limits ε_{h}; the time-delay feasible value is set as $h_{\mathrm{f}} = 0$, the time delay range is set as $h_{\max} = 0$ and $h_{\min} = 0$, and *Iter = 0*.

Step 2: Convert the given individual parameters $\boldsymbol{K}_i^g$ of the i-th controller of this generation into a matrix $\boldsymbol{K} = [\boldsymbol{D}_k \;\; \boldsymbol{C}_k; \;\; \boldsymbol{B}_k \;\; \boldsymbol{A}_k]$ and calculate $\boldsymbol{A}_{\mathrm{c}}$ and $\boldsymbol{A}_{\mathrm{dc}}$ of the closed-loop system.

Step 3: Let $h_{\mathrm{test}} = h_{\mathrm{f}} + \Delta h$; solve LMIs (6) and (7) based on the given $\boldsymbol{A}_{\mathrm{c}}$, $\boldsymbol{A}_{\mathrm{dc}}$, and h_{test}. If feasible, move to Step 4; otherwise, proceed to Step 5.

Step 4: Set $h_{\mathrm{f}} = h_{\mathrm{test}}$, $h_{\min} = h_{\mathrm{test}}$ and $h_{\mathrm{text}} = 2 \times h_{\mathrm{f}}$, then move to Step 6.

Step 5: Set $h_{\max} = h_{\mathrm{test}}$ and $h_{\mathrm{test}} = (h_{\max} + h_{\min})/2$.

Step 6: Set *Iter = Iter + 1*; if $Iter \leq Iter_{\max}$, $h_{\mathrm{gap}} = |h_{\max} - h_{\min}| \geq \varepsilon_{\mathrm{h}}$, or $h_{\mathrm{f}} \leq T_{\mathrm{dexpect}}$, return to Step 3; otherwise, proceed to Step 7.

Step 7: Output the upper limit of time delay $T_{\mathrm{dmax}} = h_{\mathrm{f}}$, and end the computation.

D. Objective Function

To apply the DE algorithm to find a better controller, the objective function $Obj(\mathrm{K})$ needs to be defined to evaluate the performance of each controller K to be selected. For time-delay control systems, the most reasonable method is to use

the MADB of the closed-loop system as the optimization objective. However, the computation of the upper bound of the time delay of the control system is very time-consuming, and if the upper bound is calculated for each selected controller, the solution process will be very long. Such a solving process would also lead to redundancies, as some randomly generated controllers are unstable when they are incorporated into closed-loop operations, even without time delay. It is also unnecessary to calculate the time delay upper bound for this part of the controllers. The stability of the closed-loop system when there is no time delay can be determined by finding the rightmost eigenvalue $\sigma_{\max}$ of the closed-loop system; the system is stable when $\sigma_{\max} < 0$. The eigenvalues of the closed-loop system can be obtained using MATLAB's eig or eigs functions, which are reliable, with high computational efficiency, and can be used for large-scale systems. Based on this, the time delay upper bounds are calculated only for controllers with $\sigma_{\max}$ smaller than 0. This can greatly reduce the number of controllers to be tested for the upper bound of the time delay and speed up the solving process.

The objective function is derived as follows.

Step 1: Find the closed-loop system without a time delay and its rightmost eigenvalue $\sigma_{\max}$.

Step 2: If $\sigma_{\max} < 0$, apply the bisection search method to iteratively check Jensen's inequality criterion and find T_{dmax} such that $Obj = -T_{\text{dmax}}$; otherwise, set $Obj = \sigma_{\max}$.

E. Controller Optimization Algorithm

In this study, we apply the mutation, crossover, and selection operations of the DE algorithm to create a new generation of controllers to be tested, providing search directions for optimizing controller performance.

1) Mutation Operation

The mutation operation generates the target individuals of the next generation by selecting three different individuals from the controller individuals of the current generation for the difference operation. The target controller individual for the mutation operation on the current generation is denoted by k_i^g (g-generation). Three different individuals ($k_{r1}^g, k_{r2}^g, k_{r3}^g$) are randomly selected from the current generation population of controllers to create the next generation of individuals $\hat{k}_i^{g+1}$ as follows:

$$\hat{k}_i^{g+1} = k_{r3}^g + \mathrm{F}(k_{r1}^g - k_{r2}^g) \tag{17}$$

where $r1$, $r2$, and $r3 \in \{1, 2, \cdots, N_{\mathrm{P}}\}$ are distinct integers that are different from the current target vector index i, thus the population size $N_{\mathrm{P}} \geq 4$. F is the scaling factor, which has values in the range of [0, 2] and is used to adjust the degree of scaling of the difference vectors.

2) Crossover Operation

The crossover operation is performed by randomly selecting two individuals (k_i^g, k_l^g) from the population of controllers of the current generation and replacing the components of k_l^g (l is a subscript index different from i) with the corresponding component in the target individual k_i^g, thus generating a new generation of individuals $\hat{k}_i^{g+1}$ to be selected. To ensure the evolution of the individuals k_i^g, at least one component of $\hat{k}_i^{g+1}$ is randomly selected from k_l^g. For the other components, the crossover probability factor CR is used to determine whether the component of $\hat{k}_i^{g+1}$ is from k_l^g or k_i^g. The crossover operation is performed as follows:

$$\hat{k}_{ij}^{g+1} = \begin{cases} k_{lj}^g, & \mathrm{rand}() \leq \mathrm{CR} \text{ or } j = \mathrm{randi}(n_v) \\ k_{ij}^g, & \mathrm{rand}() > \mathrm{CR} \text{ and } j \neq \mathrm{randi}(n_v) \end{cases} \tag{18}$$

where $\mathrm{rand}() \in [0, 1]$ is a uniformly distributed random number, j denotes the j-th variable, CR is a predetermined crossover probability constant that takes values in the range [0, 1], and $\mathrm{randi}(n_v) \in [1, 2, \cdots, n_v]$ is the index of the randomly selected dimensional variables.

3) Selection Operation

The selection operation determines whether the controller individuals generated by mutation and crossover can enter the new generation population. The test individuals k_i^g and $\hat{k}_i^{g+1}$, which are generated by mutation and crossover operations, will compete with each other; when the fitness value of $\hat{k}_i^{g+1}$ is equal to or better than k_i^g, it will be selected as the new generation individual k_i^{g+1}; otherwise, k_i^g is selected directly as the offspring.

$$k_i^{g+1} = \begin{cases} \hat{k}_i^{g+1}, & \mathrm{Obj}(\hat{k}_i^{g+1}) \leq \mathrm{Obj}(k_i^g) \\ k_i^g, & \mathrm{Obj}(\hat{k}_i^{g+1}) > \mathrm{Obj}(k_i^g) \end{cases} \tag{19}$$

IV. Algorithm Flow

Based on the above ideas and results, the complete steps of the time-delay stability synthesis algorithm for power systems using Jensen's integral inequality and the DE-LMI are shown in Fig. 1.

Step 1: Input power system model state-space model parameters $\boldsymbol{A}$, $\boldsymbol{B}$, $\boldsymbol{C}$, $\boldsymbol{D}$; set the dimensions of input and output signal n_u, n_y; set controller orders n_k; set number of decision variables $n_v = (n_u + n_k) \times (n_y + n_k)$; initialize DE parameters (including scaling factor CF, crossover probability CR, population size N_{P}); set maximum number of iterations $g_{\max}$ and iteration error limits ε; set $g = 1$.

Step 2: Randomly generate the initial population $\boldsymbol{K} \in \boldsymbol{R}^{N_p \times \mathrm{I_d}}$ of controllers $\boldsymbol{K}_s$, whose i-th row vector $\boldsymbol{K}_i$ represents the i-th controller individual.

Step 3: Transform the N_{P} individuals $\boldsymbol{K}_i$ into the controller state-space matrix $\boldsymbol{K}_{\mathrm{s_}i}$ and generate the closed-loop system matrix $\boldsymbol{A}_{\mathrm{c}i}$, $\boldsymbol{B}_{\mathrm{c}i}$, $\boldsymbol{C}_{\mathrm{c}i}$, and $\boldsymbol{D}_{\mathrm{c}i}$ without time delay.

Step 4: Check whether the rightmost eigenvalue of each $\boldsymbol{A}_{\mathrm{c}i}$ lies in the left half-plane; if so, proceed to Step 5; if none of the $\boldsymbol{A}_{\mathrm{c}i}$ of the N_{P} individuals in this generation satisfy this, return to Step 2.

Step 5: Using Jensen's inequality criterion with the bisection search method, compute the MADB $T_{\text{dmax_}i}$ corresponding to each individual. Obtain the optimal individual of this generation, $\boldsymbol{K}_{\text{best}}^g$ and T_{dmax}^g.

Step 6: Perform crossover, mutation, and selection operations among the N_{P} individuals in the current generation to create the next generation of individuals K_i^{g+1}, and set $g = g + 1$.

Step 7: If $g \leq g_{\max}$ or $|T_{\text{dmax}}^{g+1} - T_{\text{dmax}}^g| \geq \varepsilon$, return to Step 3; otherwise, proceed to Step 8.

Step 8: Output the optimal solution T^g_{dmax} and the corresponding controller matrix $\boldsymbol{K}^g_{\text{best}}$ and end the computation.

V. Case Study

A. Case 1: Single Machine Infinite Bus System

The effectiveness of the method is verified using a single machine against an infinite bus system. The wiring diagram and parameters can be found in [26]. The case can be described by the following fourth-order state-space equation, with the following system matrices:

$$\boldsymbol{A} = \begin{bmatrix} 0 & 314.00 & 0 & 0 \\ -0.1445 & 0 & -0.0976 & 0 \\ -0.2082 & 0 & -0.4633 & 0.1667 \\ 34.0970 & 0 & -525.4400 & -20.00 \end{bmatrix} \tag{20}$$

$$\boldsymbol{B} = \begin{bmatrix} 0 \\ 0 \\ 0 \\ 1000 \end{bmatrix}, \quad \boldsymbol{C} = \begin{bmatrix} 1 & 0 & 0 & 0 \\ 0 & 1 & 0 & 0 \end{bmatrix} \tag{21}$$

When no control is applied, the following weak damped oscillation mode exists in the system: $-0.0207 \pm 4.7609\text{i}$, with a damping ratio of approximately 0.4350% and an oscillation frequency of 0.7577 Hz. The controller design goal is to maximize the allowable delay bound of the closed-loop system with the output signal transmission time delay (assuming a time-delay rate of change $\mu = 0.001$).

A SOF controller and a 4-th order DOF controller were designed using the FWM method and the proposed Jensen's method, respectively. The parameters used in the test for Jensen's method are as follows: DE algorithm population size $N_p = 40$, number of decision variables $N_v = 2$, scaling factor F = 0.85, crossover probability CR = 1.0, maximum population size $g_{\max} = 20$, iterations number of bisection search method *Iter*_max = 10, and error limit $\varepsilon = 0.001$. The maximum number of iterations for the FWM method is set to 20. The test computer is equipped with an Intel i7-6500U CPU at 2 × 2.50 GHz and 8.00 GB of memory.

To verify the actual MADB value of the closed-loop system, the corresponding system models are established in Simulink, and the MADB is calibrated using time-domain simulations using the time-delay scanning method. All the results of the controller performance analysis are shown in Table I.

As can be seen from Table I, Jensen's method requires 4.6494 s and 148.4590 s to find the static and 4-th order dynamic output-feedback controllers, respectively, while the FWM method requires 139.4592 s and 830.3688 s, respectively. Moreover, the computation time required for the Jensen's method is only 3.3–17.9% of that for the FWM method, thereby exhibiting an advantage in terms of computational efficiency. For the upper limit of the allowed time-delay estimation, the static and dynamic controllers given by the Jensen's method are 0.1406 s and 0.1667 s, respectively, while those given by the FWM method are 0.1563 s and 0.1875 s, respectively, indicating that the estimation accuracy of the FWM method is higher than that of the Jensen's method.

It can also be seen from Table I that when a static output controller designed via the Jensen's method is applied, the MADB of the closed-loop system estimated by Jensen's method and time-domain simulation is 0.1406 s and 0.2050 s, respectively, indicating that the estimation accuracy of the Jensen's method is approximately 68.58%. With a 4-th order DOF controller, the MADB estimated by the Jensen's method and time-domain simulation is approximately 0.1667 s and 0.2560 s, respectively, with an estimated accuracy of approximately 65.12%.

As for the FWM method, when a static output controller designed via it is applied, the MADB given by the FWM method and time-domain simulation is 0.1563 s and 0.2010 s, respectively, indicating that the estimation accuracy of the FWM method is approximately 77.76%. When a 4-th order DOF controller is used, the MADB estimated by the FWM method and time-domain simulation method is approximately 0.1875 s and 0.2460 s, respectively, with an estimated accuracy of approximately 76.22%.

The closed-loop system outputs of the 4-th order DOF controllers designed using the Jensen's method and the FWM method at different input time delays are shown in Figs. B1 and B2 in Appendix B. From the figures, it can be seen that when the controller designed via Jensen's method is applied, the system oscillations are quickly smoothed out and the system damping is greatly improved when there is no transmission time delay or a small transmission time delay ($T_{\text{d}} \leq 0.1$ s) in the output signal of the controllers. For the controller designed via the FWM method, the output is weakly damped even when $T_{\text{d}} \leq 0.1$ s. Apparently, the controllers designed using the Jensen's method achieves a more excellent performance.

It can be concluded from this implementation that although the Jensen's method is less accurate than the FWM method for estimating the MADB, it requires fewer decision variables, is more than five times faster than the FWM method and, ultimately, has better performance than the FWM method because more potential allowable time-delay upper bounds of the controllers can be tested in a short time period.

B. Case 2: Time Delay Stability Synthesis of a 4-machine 2-area 1-DC System

The test system is the well-known 4-machine 2-area system,

TABLE I
Comparison of Controller Performance of Case 1

Od	Jensen's Method			FWM Method		
n_k	MADB_c (s)	MADB_v (s)	Comp Time (s)	MADB_c (s)	MADB_v (s)	Comp Time (s)
0	0.1406	0.2050	4.6494	0.1563	0.2010	139.4592
4	0.1667	0.2560	148.4590	0.1875	0.2460	830.3688

Note: Od = Order of controller; MADB_c = computation value of MADB; MADB_v = verified value of MADB; CompTime = computation time.

which is designed following the procedure reported in [27]. The final system structure is shown in Fig. 2. The effect of the time delay on the system stability can be observed by applying a time delay at the output of the HVDC supplementary controller. The following fault is applied to verify the controller performance: a three-phase short-circuit ground fault is applied at bus 8 at 1 s, and the breakers on both sides of one of the lines from bus 8 to bus 9 are tripped at 1.1 s.

A 9-th order state-space model is obtained by the system identification method. Two weakly damped oscillation modes exist in the open-loop system: $-0.0207 \pm 4.7609\mathrm{i}$ with a damping ratio of approximately 0.4350% and an oscillation frequency of 0.7577 Hz. The MADB was calculated for Case 2 using both the proposed method and the FWM method. The Case 2 model was also established in Simulink and the time delay was gradually increased in steps of 10 ms at the output signal of the controller to observe the stability of the system after the fault was applied. The corresponding calculation results are presented in Table II.

From Table II, it can be seen that when a static output controller is used, the MADB provided by the FWM method and time-domain simulation is 0.3000 s and 0.3427 s, respectively, with an estimated accuracy of approximately 87.54%. When a 3rd-order dynamic output controller is used, the MADB provided by the FWM method and time-domain simulation is 0.4500 s and 0.4939 s, respectively, with an estimated accuracy of approximately 91.11%.

When a static output controller is used, the upper limit of the time delay presented by the FWM method and time-domain simulation is 0.3000 s and 0.3970 s, respectively, with an estimation accuracy of approximately 80.50%. When a dynamic output controller of order 3 is used, the upper limit of time delay given by the FWM method and time-domain simulation is 0.4500 s and 0.5030 s, respectively, with an estimation accuracy of approximately 89.46%.

Figure 3 shows the closed-loop system output results of the controller proposed in this study for different time delays. These results reveal that the stability of the system with output signal time delays is significantly improved by the method established in this study. Furthermore, both methods can evidently be used to design controllers that can endure longer signal transmission time delays. The FWM method is more accurate and less conservative in estimating the upper bounds of time delay, but it is much more computationally intensive than the Jensen's method. For the time delay controllers with the same order, the FWM method gives better estimations of MADB than the Jensen's method in this case. However, when we check the estimation value given by the two methods via the time domain simulation method, it shows that the Jensen's method achieves a higher MADB.

C. Case 3: Time-Delay Stability Synthesis of 29-bus 7-machine 3-DC System

This case was established, as reported in [28], with the Canadian 735 kV equivalent network, which is a pure AC system with 29 buses and 7 machines, with a 26,200 MW system unit capacity and 23,000 MW load. This system contains multiple components, including series compensation, high-voltage resistance, and wind power. It is a typical 2-sender 2-receiver system, similar to the grid structure of the China Southern Grid and Brazil Grid. To study the effect of the proposed method on the hybrid AC/DC system, three HVDC circuits were added to the original network, with the following specifications and locations (see Fig. 4): i) $\pm$ 500 kV/1000 MW between bus LG27 and bus MTL7; ii) $\pm$ 500 kV/500 MW between bus CHU7 and bus QUE7; iii) $\pm$ 500 kV/500 MW between bus CHU7 and bus QUE7.

The relative angular speed output vectors U of units G4, G6, and G7 were obtained by adding a random perturbation signal vector Y at each DC, and the 16th order state-space

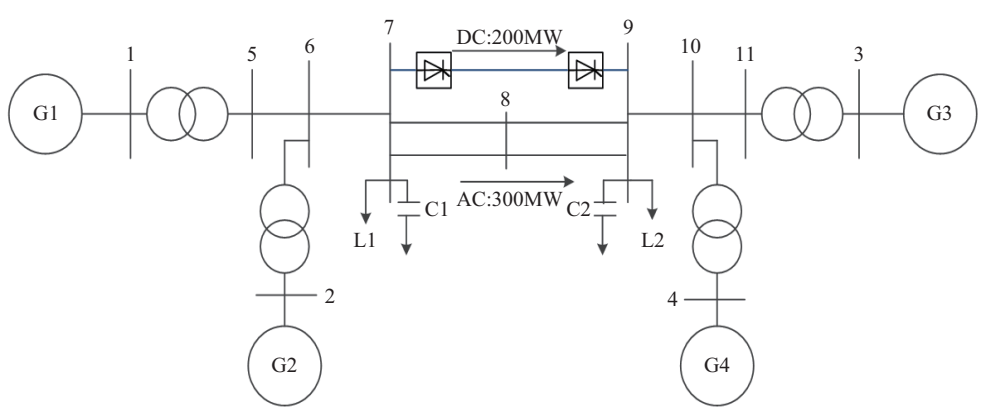

Fig. 2. Schematic of the 4-machine-2-area-1-DC hybrid system used in this study.

TABLE II
COMPARISON OF CONTROLLER PERFORMANCE OF CASE 2

Od	Jensen's Method			FWM Method		
n_k	MADB_c/s	MADB_v/s	Comp.Time/s	MADB_c/s	MADB_v/s	Comp. Time/s
0	0.3000	0.3970	1.3311	0.3427	0.3870	153.2881
3	0.4500	0.5030	9.6533	0.4500	0.4940	1869.6581

Note: Od = Order of controller; MADB_c = computation value of MADB; MADB_v = verified value of MADB; CompTime = computation time.

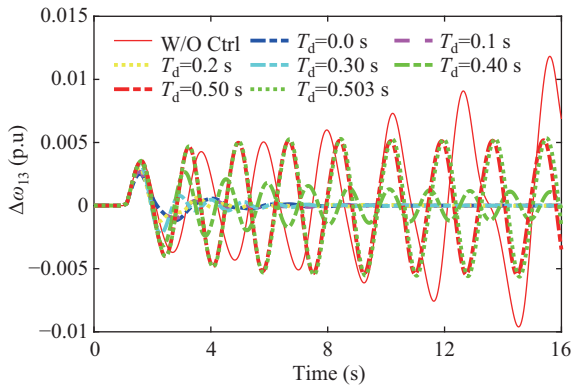

Fig. 3. Time-domain simulation results of DOF controller obtained using Jensen's method (Case 2).

equations with three inputs and three outputs were obtained via the identification method.

When there is no supplement control applied to the HVDCs, the rightmost pole of the system is $-0.1669\pm4.3574i$, which is a weakly damped oscillatory mode, with a damping ratio of 3.83% and a frequency of 0.6935 Hz.

The Jensen's method and the FWM method were used to design the 16-th DOF time-delay stabilization controller, and the results are presented in Table III. For this 16-th order system, the FWM method was unable to find a convergent solution after multiple attempts.

TABLE III
DOF CONTROLLER DESIGN RESULT IN CASE 3

Method	MADB/s	CompTime	Check
Jensen	0.6100	3056.0374	0.8000
FWM		Fail	

In contrast, the Jensen's method found a controller with an MADB of 0.6100 s on the time delay after 3056.0374 s, and the time-domain simulation verified the upper bound of 0.8000 s.

Fig. B3 in Appendix B shows the angular speed of the closed-loop system units G1, G4, and G7 for different time delays with the controller proposed in this study. From Fig. 9(a) and (b), it can be seen that the designed controller significantly improves the stability of the system in the presence of a time delay in the input signal, and the disturbance to the system by the fault is smoothed out more quickly than the condition without controller.

Table IV presents the results of the system damping ratio based on the angular speed signals of units for the closed-loop system with different time delays by applying the TLS-ESPRIT method. It is evident from the table that the damping ratio of the closed-loop system decreases as the time delay increases, and when the time delay is increased to 0.5000 s, the damping of the closed-loop system is essentially the same

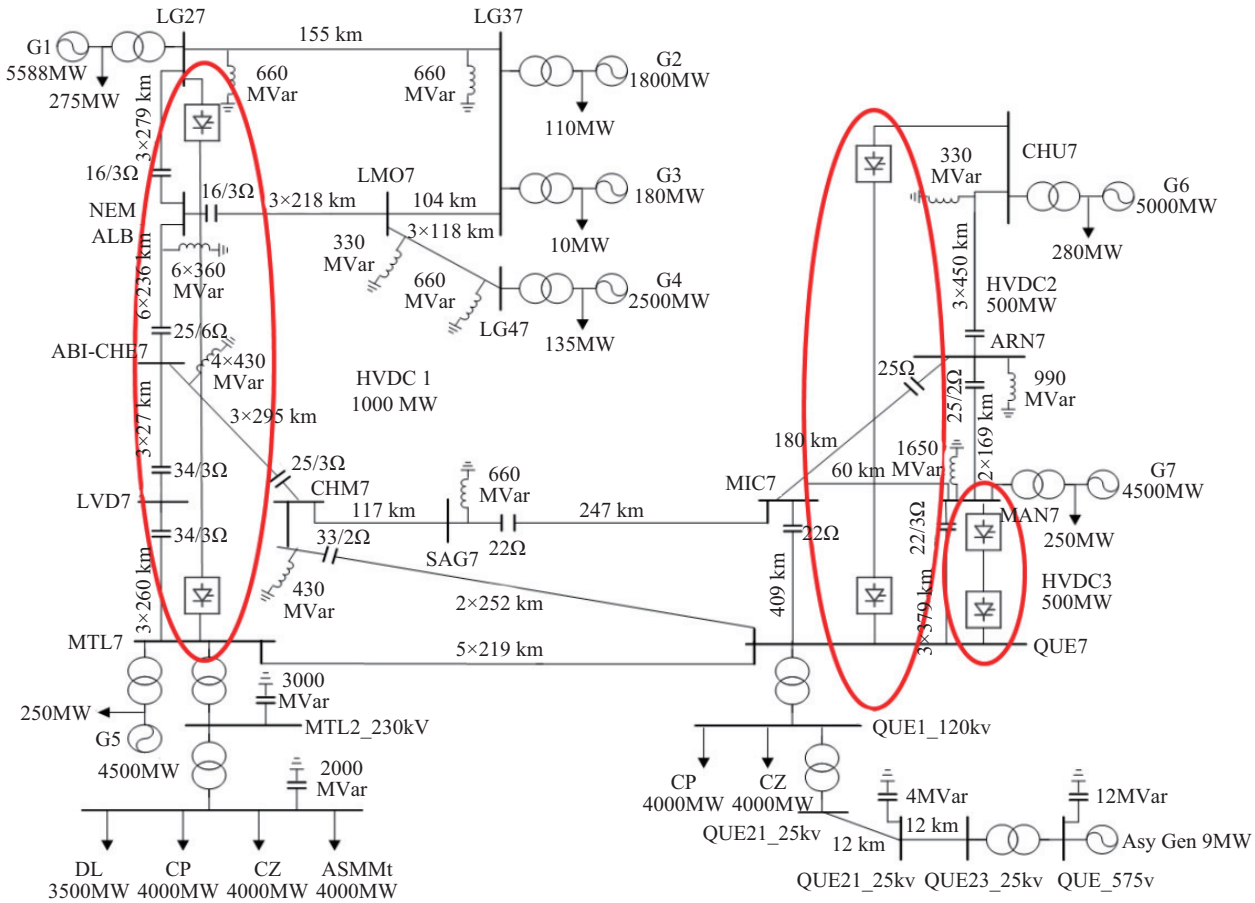

Fig. 4. Schematic of the 29-bus7- machine 3-DC system used in this study.

TABLE IV
EFFECT OF TIME DELAY ON DAMPING OF CLOSED-LOOP SYSTEM

Time delay (s)	Damping ratio	Time delay (s)	Damping ratio
0	10.97%	0.5000	3.50%
0.1000	10.72%	0.6000	2.10%
0.2000	9.39%	0.7000	1.21%
0.3000	8.92%	0.800	0.50%
0.4000	6.65%	–	

as that of the open-loop system. As the time delay continues to increase, the controller negatively affects the performance of the closed-loop system. When the time delay exceeds 0.8000 s, the damping ratio of the closed-loop system becomes lower than that of the open-loop, and the angular speed signals start to oscillate. As the time delay increases further, the oscillations increase, and the system loses stability. The simulation results indicate that the controller designed based on the Jensen's method has strong anti-delay ability.

VI. CONCLUSION

A time-delay-dependent wide-area damping controller synthesis approach, which is based on the delay-stability criterion via Jensen's inequality, and using the DE and LMI hybrid algorithms as the solution tool, is developed in this study. The method is characterized by fewer decision variables and greater computation efficiency, achieving a higher upper limit of delay stability than that of FWM method. The examples show that the proposed method can be applied to large-scale delay systems, especially for controller synthesis controlling high-dimensional systems, such as the wide-area control of power systems. Based on the DE-LMI hybrid solution framework, the method can also be extended to the H_∞ and H_2 synthesis of the delay system.

APPENDIX

A. Proof of Lemma 2

PROOF: The Lyapunov function is defined as:

$$V(\boldsymbol{x}_t) = \boldsymbol{x}^{\mathrm{T}}(t)\boldsymbol{P}\boldsymbol{x}(t) + \int_{t-\mathrm{d}(t)}^{t} \boldsymbol{x}^{\mathrm{T}}(s)\boldsymbol{Q}\boldsymbol{x}(s)\mathrm{d}s + \int_{t-h}^{t} \boldsymbol{x}^{\mathrm{T}}(s)\boldsymbol{S}\boldsymbol{x}(s)\mathrm{d}s + \int_{-h}^{0}\int_{t+\theta}^{t} h\dot{\boldsymbol{x}}^{\mathrm{T}}(s)\boldsymbol{V}\dot{\boldsymbol{x}}(s)\mathrm{d}s\mathrm{d}\theta \tag{A1}$$

In the above equations, $\boldsymbol{x}_t = \boldsymbol{x}(t+\theta)$ and $-2h \le \theta \le 0$. The derivative of the Lyapunov function of the above equation yields:

$$\begin{aligned}\dot{V}(\boldsymbol{x}_t) = {} & 2\boldsymbol{x}(t)^{\mathrm{T}}\boldsymbol{P}(\boldsymbol{A}\boldsymbol{x}(t) + \boldsymbol{A}_{\mathrm{d}}\boldsymbol{x}(t-\mathrm{d}(t)) + \boldsymbol{x}(t)^{\mathrm{T}}\boldsymbol{Q}\boldsymbol{x}(t) \\ & + \boldsymbol{x}(t)^{\mathrm{T}}\boldsymbol{S}\boldsymbol{x}(t) - (1-u)\boldsymbol{x}(t-\mathrm{d}(t))^{\mathrm{T}}\boldsymbol{Q}\boldsymbol{x}(t-\mathrm{d}(t)) \\ & - \boldsymbol{x}(t-h)^{\mathrm{T}}\boldsymbol{S}\boldsymbol{x}(t-h) + (\boldsymbol{A}x(t) \\ & + \boldsymbol{A}_{\mathrm{d}}\boldsymbol{x}(t-\mathrm{d}(t))^{\mathrm{T}}(h^2\boldsymbol{V})(\boldsymbol{A}\boldsymbol{x}(t) + \boldsymbol{A}_{\mathrm{d}}\boldsymbol{x}(t-\mathrm{d}(t)) \\ & - \int_{t-h_2}^{t} h\dot{\boldsymbol{x}}(t)^{\mathrm{T}}\boldsymbol{V}\dot{\boldsymbol{x}}(t)\mathrm{d}t \end{aligned} \tag{A2}$$

where

$$\begin{aligned} & -\int_{t-h}^{t} h\dot{\boldsymbol{x}}(t)^{\mathrm{T}}\boldsymbol{V}\dot{\boldsymbol{x}}(t)\mathrm{d}t = \\ & -\int_{t-h}^{t-\mathrm{d}(t)} (h-\mathrm{d}(t))\dot{\boldsymbol{x}}(t)^{\mathrm{T}}\boldsymbol{V}\dot{\boldsymbol{x}}(t)\mathrm{d}t \\ & -\int_{t-h}^{t-\mathrm{d}(t)} \mathrm{d}(t)\dot{\boldsymbol{x}}(t)^{\mathrm{T}}\boldsymbol{V}\dot{\boldsymbol{x}}(t)\mathrm{d}t \\ & -\int_{t-\mathrm{d}(t)}^{t} \mathrm{d}(t)\dot{\boldsymbol{x}}(t)^{\mathrm{T}}\boldsymbol{V}\dot{\boldsymbol{x}}(t)\mathrm{d}t \\ & -\int_{t-\mathrm{d}(t)}^{t} (h-\mathrm{d}(t))\dot{\boldsymbol{x}}(t)^{\mathrm{T}}\boldsymbol{V}\dot{x}(t)\mathrm{d}t \end{aligned} \tag{A3}$$

Let $\beta = \mathrm{d}(t)/h$, then

$$\begin{aligned} & -\int_{t-h}^{t-\mathrm{d}(t)} \mathrm{d}(t)\dot{\boldsymbol{x}}(t)^{\mathrm{T}}\boldsymbol{V}\dot{\boldsymbol{x}}(t)\mathrm{d}t \\ & = -\beta\int_{t-h}^{t-\mathrm{d}(t)} h\dot{\boldsymbol{x}}(t)^{\mathrm{T}}\boldsymbol{V}\dot{\boldsymbol{x}}(t)\mathrm{d}t \\ & \le -\beta\int_{t-h}^{t-\mathrm{d}(t)} h-\mathrm{d}(t))\dot{\boldsymbol{x}}(t)^{\mathrm{T}}\boldsymbol{V}\dot{\boldsymbol{x}}(t)\mathrm{d}t \end{aligned} \tag{A4}$$

Furthermore,

$$\begin{aligned} & -\int_{t-\mathrm{d}(t)}^{t} h-\mathrm{d}(t))\dot{x}(t)^{\mathrm{T}}V\dot{x}(t)\mathrm{d}t \\ & = -(1-\beta)\int_{t-\mathrm{d}(t)}^{t} h\dot{x}(t)^{\mathrm{T}}V\dot{x}(t)\mathrm{d}t \\ & \le -(1-\beta)\int_{t-\mathrm{d}(t)}^{t} d(t)\dot{x}(t)^{\mathrm{T}}V\dot{x}(t)\mathrm{d}t \end{aligned} \tag{A5}$$

From Lemma 1,

$$\begin{aligned} & -\int_{t-h}^{t} h\dot{\boldsymbol{x}}(t)^{\mathrm{T}}\boldsymbol{V}\dot{\boldsymbol{x}}(t)\mathrm{d}t \le \\ & -(\boldsymbol{x}(t-\mathrm{d}(t)) - \boldsymbol{x}(t-h))^{\mathrm{T}}\boldsymbol{V}(\boldsymbol{x}(t-\mathrm{d}(t)) - \boldsymbol{x}(t-h)) \\ & -(\boldsymbol{x}(t) - \boldsymbol{x}(t-\mathrm{d}(t)))^{\mathrm{T}}\boldsymbol{V}(\boldsymbol{x}(t) - \boldsymbol{x}(t-\mathrm{d}(t))) \\ & -\beta(\boldsymbol{x}(t-\mathrm{d}(t)) - \boldsymbol{x}(t-h))^{\mathrm{T}}\boldsymbol{V}(\boldsymbol{x}(t-\mathrm{d}(t)) - \boldsymbol{x}(t-h)) \\ & -(1-\beta)(\boldsymbol{x}(t) - \boldsymbol{x}(t-\mathrm{d}(t)))^{\mathrm{T}}\boldsymbol{V}(\boldsymbol{x}(t) - \boldsymbol{x}(t-\mathrm{d}(t))) \end{aligned} \tag{A6}$$

From (A1)–(A6), we have

$$\begin{aligned} & \dot{V}(x_t) \le \\ & \boldsymbol{x}(t)^{\mathrm{T}}\left[\boldsymbol{P}\boldsymbol{A} + \boldsymbol{A}^{\mathrm{T}}\boldsymbol{P} + \boldsymbol{Q} + \boldsymbol{S} + \boldsymbol{A}^{\mathrm{T}}(h^2\boldsymbol{V})\boldsymbol{A}\right]\boldsymbol{x}(t) \\ & \quad + 2\boldsymbol{x}(t)^{\mathrm{T}}\left[\boldsymbol{P}\boldsymbol{A}_{\mathrm{d}} + \boldsymbol{A}^{\mathrm{T}}\boldsymbol{P} + \boldsymbol{A}^{\mathrm{T}}(h^2\boldsymbol{V})\boldsymbol{A}_{\mathrm{d}}\right]\boldsymbol{x}(t-\mathrm{d}(t)) \\ & \quad + \boldsymbol{x}(t-\mathrm{d}(t))^{\mathrm{T}}\left[-(1-\mu)\boldsymbol{Q} - 2\boldsymbol{V} + \boldsymbol{A}_{\mathrm{d}}^{\mathrm{T}}(h^2\boldsymbol{V})\boldsymbol{A}_{\mathrm{d}}\right] \\ & \qquad \cdot \boldsymbol{x}(t-\mathrm{d}(t)) \\ & \quad + 2\boldsymbol{x}(t-\mathrm{d}(t))^{\mathrm{T}}\boldsymbol{V}\boldsymbol{x}(t) + 2\boldsymbol{x}(t-\mathrm{d}(t))^{\mathrm{T}}\boldsymbol{V}\boldsymbol{x}(t-h) \\ & \quad - \boldsymbol{x}(t)^{\mathrm{T}}(\boldsymbol{V})x(t) - \boldsymbol{x}(t-h)^{\mathrm{T}}(\boldsymbol{S}+\boldsymbol{V})\boldsymbol{x}(t-h) \\ & \quad - \beta(\boldsymbol{x}(t-\mathrm{d}(t)) - \boldsymbol{x}(t-h))^{\mathrm{T}}\boldsymbol{V}(\boldsymbol{x}(t-\mathrm{d}(t)) - \boldsymbol{x}(t-h)) \\ & \quad - (1-\beta)(\boldsymbol{x}(t) - \boldsymbol{x}(t-\mathrm{d}(t)))^{\mathrm{T}}\boldsymbol{V}(\boldsymbol{x}(t) - \boldsymbol{x}(t-\mathrm{d}(t))) \\ & = \boldsymbol{\zeta}(t)^{\mathrm{T}}\boldsymbol{\Psi}\boldsymbol{\zeta}(t) - \beta(\boldsymbol{x}(t-\mathrm{d}(t)) - \boldsymbol{x}(t-h))^{\mathrm{T}} \\ & \quad \cdot \boldsymbol{V}(\boldsymbol{x}(t-\mathrm{d}(t)) - \boldsymbol{x}(t-h)) \\ & \quad - (1-\beta)(\boldsymbol{x}(t) - \boldsymbol{x}(t-\mathrm{d}(t)))^{\mathrm{T}}\boldsymbol{V}(\boldsymbol{x}(t) - \boldsymbol{x}(t-\mathrm{d}(t))) \\ & = \boldsymbol{\zeta}(t)^{\mathrm{T}}[(1-\beta)\boldsymbol{\Psi}_1 + \beta\boldsymbol{\Psi}_2]\boldsymbol{\zeta}(t) \end{aligned} \tag{A7}$$

The definition of the above equation Ψ, Ψ_1, and Ψ_2 are described in Lemma 2.

We can also write:

$$\boldsymbol{\zeta}(t) = \left[\boldsymbol{x}(t)^{\mathrm{T}} \quad \boldsymbol{x}(t-\mathrm{d}(t))^{\mathrm{T}} \quad \boldsymbol{x}(t-h)^{\mathrm{T}}\right] \tag{A8}$$

Because $0 \leq \beta \leq 1$, the derivative of the energy function in $(1-\beta)\boldsymbol{\Psi}_1 + \beta\boldsymbol{\Psi}_2$ is a convex combination. Thus, it can be concluded that the system is asymptotically stable when $\boldsymbol{\Psi}_1$ and $\boldsymbol{\Psi}_2$ are negative.

B. Attached Figures

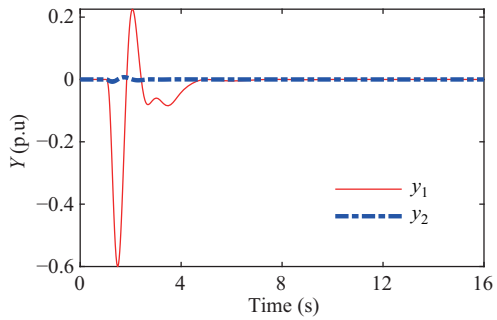

(a) $T_{\mathrm{d}} = 0.0$ s

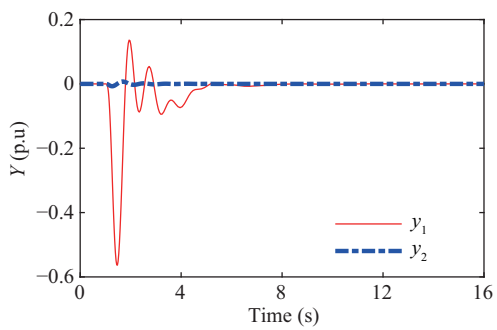

(b) $T_{\mathrm{d}} = 0.1$ s

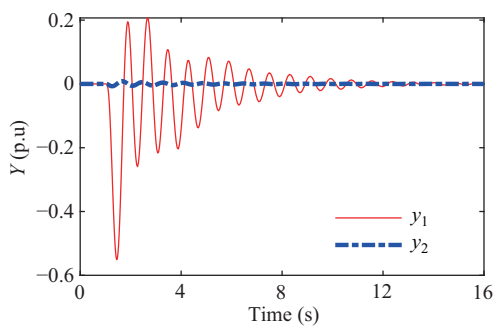

(c) $T_{\mathrm{d}} = 0.2$ s

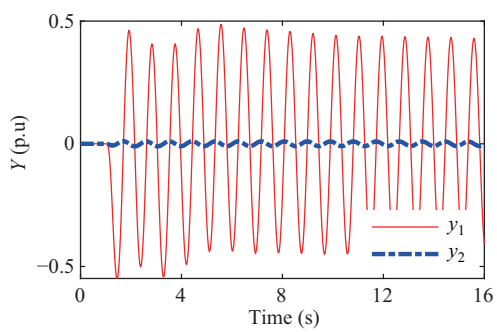

(d) $T_{\mathrm{d}} = 0.25$ s

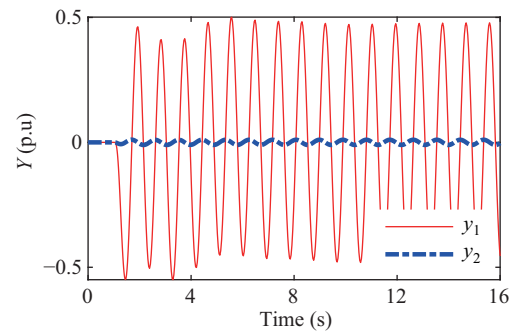

(e) $T_{\mathrm{d}} = 0.2560$ s

Fig. B1. Time-domain simulation results of the 4th order DOF controller obtained using Jensen's method (Case 1).

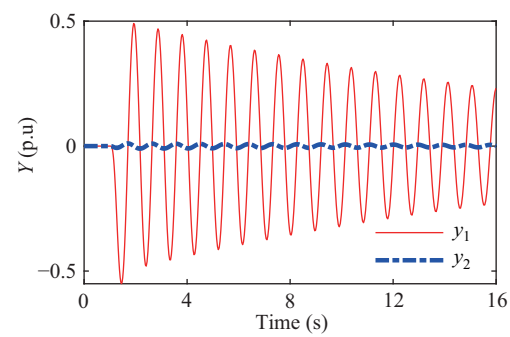

(a) $T_{\mathrm{d}} = 0.0$ s

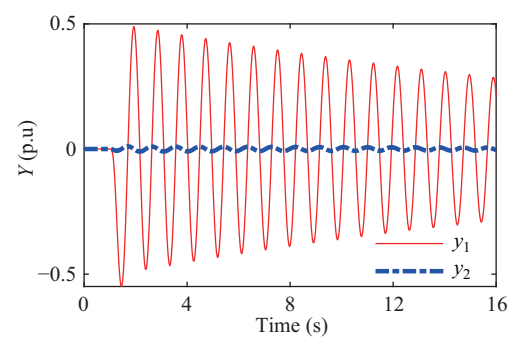

(b) $T_{\mathrm{d}} = 0.1$ s

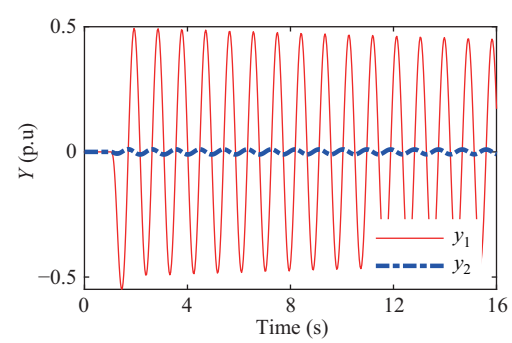

(c) $T_{\mathrm{d}} = 0.2$ s

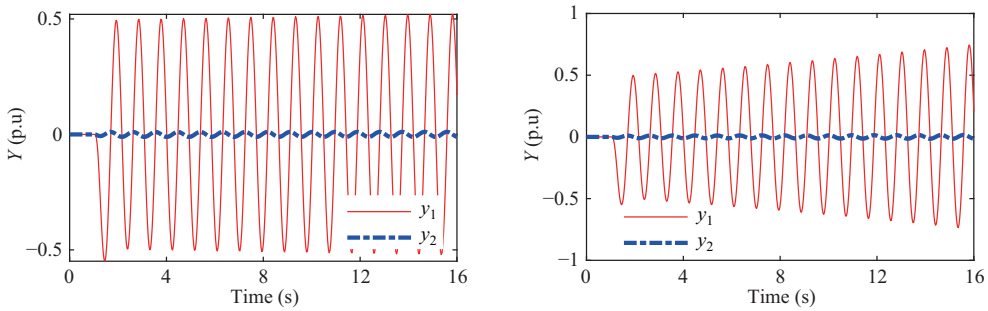

(d) $T_{\mathrm{d}} = 0.2460$ s (e) $T_{\mathrm{d}} = 0.25$ s

Fig. B2. Time-domain simulation results of the 4th order DOF based on the FWM method (Case 1).

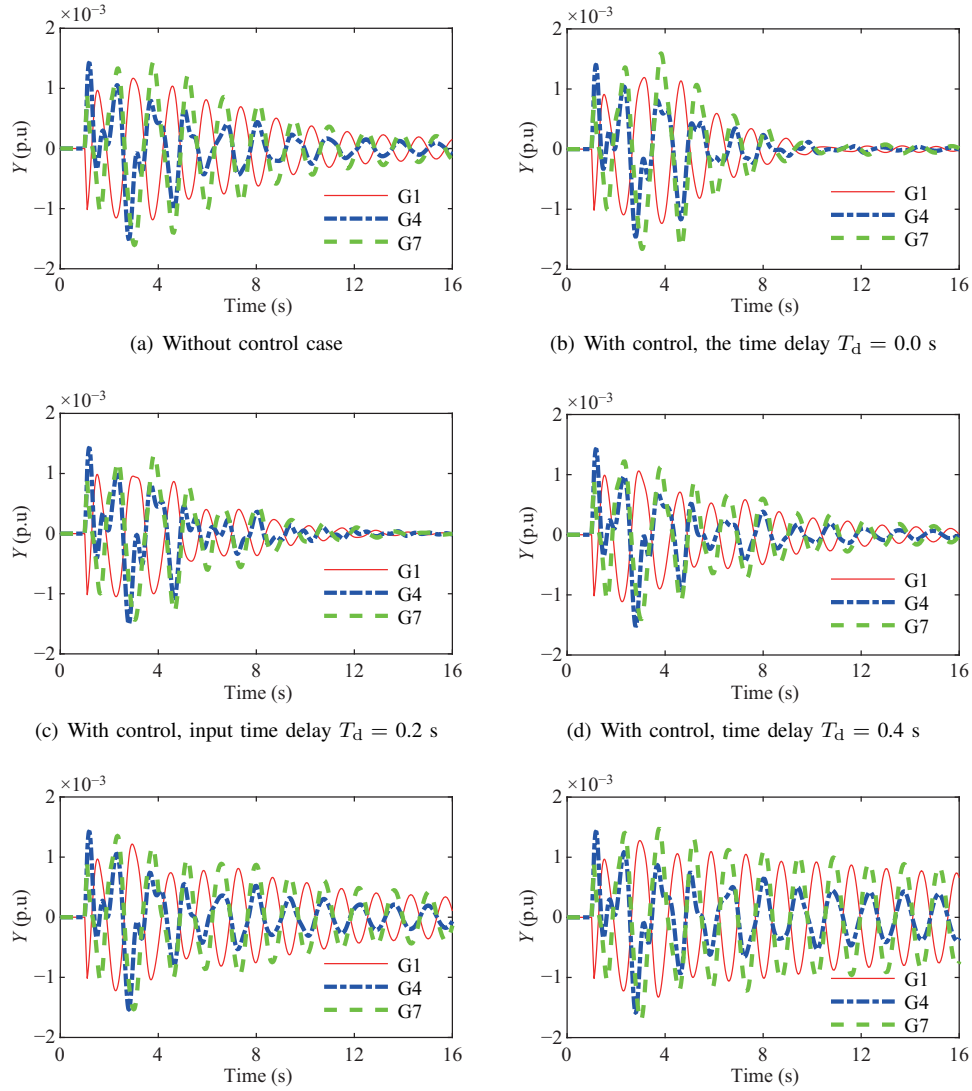

(a) Without control case (b) With control, the time delay $T_{\mathrm{d}} = 0.0$ s

(c) With control, input time delay $T_{\mathrm{d}} = 0.2$ s (d) With control, time delay $T_{\mathrm{d}} = 0.4$ s

(e) With Control, input time delay $T_{\mathrm{d}} = 0.50$ s (f) With Control, input time delay $T_{\mathrm{d}} = 0.8$ s

Fig. B3. Time-domain simulation results of DOF controller based on Jensen's method (Case 3).

REFERENCES

[1] T. Wang, C. C. Li, D. K. Mi, Z. P. Wang, and Y. W. Xiang, "Coordinated modulation strategy considering multi-HVDC emergency for enhancing transient stability of hybrid AC/DC power systems," *CSEE Journal of Power and Energy Systems*, vol. 6, no. 4, pp. 806–815, Dec. 2020, doi: 10.17775/CSEEJPES.2019.02000.

[2] X. L. Liu, S. D. Zhang, X. H. Zeng, L. Yao, Y. J. Ding, and C. H. Deng, "Evaluating the network communication delay with WAMS for multi-energy complementary systems," *CSEE Journal of Power and Energy Systems*, vol. 6, no. 2, pp. 402–409, Jun. 2020.

[3] C. Zhang, "Design and simulation of separate broadcast control architecture of satellite delay tolerant network for mass sensors," *Journal of Physics: Conference Series*, vol. 1169, no. 1, pp. 012069, Feb. 2019,

doi: 10.1088/1742-6596/1169/1/012069.

[4] L. Zhang, Z. B. Zhan, L. P. Wei, B. N. Shi, and X. D. Xie, "Test and analysis of piecewise delay in wide area measurement system," *Automation of Electric Power Systems*, vol. 40, no. 6, pp. 101–106, Mar. 2016, doi: 10.7500/AEPS20150427008.

[5] G. Duan, Y. Q. Yan, X. D. Xie, H. Z. Tao, D. Yang, L. D. Wang, K. Zhao, and J. S. Li, "Development status quo and tendency of wide area phasor measuring technology," *Automation of Electric Power Systems*, vol.39, no. 1, pp. 73–80, Jan. 2015, doi: 10.7500/AEPS20141008016.

[6] S. D. Xu, H. Liu, and T. S. Bi, "Reference phasor calculation method for calibrator of synchronous phasor measurement unit," *Automation of Electric Power Systems*, vol. 43, no. 17, pp. 168–175, Sep. 2019, doi: 10.7500/AEPS20180723018.

[7] C. Ziras, E. Vrettos, and S. You, "Controllability and stability of primary frequency control from thermostatic loads with delays," *Journal of Modern Power Systems and Clean Energy*, vol. 5, no. 1, pp. 43–54, Jan. 2017.

[8] M. Xiao, Q. Mo, P. Li, and K. Zhang, "Operation and evaluation of the coordinated HVDC damping control system of China Southern Power Grid," *Southern Power System Technology*, vol. 4, no. 3, pp. 42–46, Jun. 2010, doi: 10.3969/j.issn.1674-0629.2010.03.009.

[9] J. Sieber, K. Engelborghs, T. Luzyanina, G. Samaey, and D. Roose. (2016, Sep.). DDE-BIFTOOL Manual-Bifurcation analysis of delay differential equations. *Mathematics*. [Online]. Available: https://arxiv.org/abs/1406.7144.

[10] Z. Wu and W. Michiels, "Reliably computing all characteristic roots of delay differential equations in a given right half plane using a spectral method," *Journal of Computational and Applied Mathematics*, vol. 236, no. 9, pp. 2499–2514, Mar. 2012.

[11] B. Pal and B. Chaudhuri, *Robust Control in Power Systems*, Boston, MA: Springer, 2006.

[12] W. Michiels and S. Gumussoy. (2014). Eigenvalue Based Algorithms and Software for the Design of Fixed-Order Stabilizing Controllers for Interconnected Systems with Time-Delays. [Online]. Available: https://arxiv.org/abs/2003.05496v2.

[13] Y. He, M. Wu, G. P. Liu, and J. H. She, "Output feedback stabilization for a discrete-time system with a time-varying delay," *IEEE Transactions on Automatic Control*, vol. 53, no. 10, pp. 2372–2377, Nov. 2008.

[14] M. Wu, Y. He, and J. H. She, *Stability Analysis and Robust Control of Time-Delay Systems*, Beijing: Science Press, 2010.

[15] J. Ma, J. C. Li, X. Gao, and Z. P. Wang, "Research on time-delay stability upper bound of power system wide-area damping controllers based on improved free-weighting matrices and generalized eigenvalue problem," *International Journal of Electrical Power & Energy Systems*, vol. 64, pp. 476–482, Jan. 2015.

[16] Y. Li, C. Rehtanz, D. Yang, S. Rüberg, and U. Häger, "Robust high-voltage direct current stabilising control using wide-area measurement and taking transmission time delay into consideration," *IET Generation, Transmission & Distribution*, vol. 5, no. 3, pp. 289–297, Apr. 2011.

[17] Y. Li, Y. Zhou, F. Liu, Y. J. Cao, and C. Rehtanz, "Design and implementation of delay-dependent wide-area damping control for stability enhancement of power systems," *IEEE Transactions on Smart Grid*, vol. 8, no. 4, pp. 1831–1842, Jul. 2017.

[18] K. Q. Gu, V. L Kharitonov, and J. Chen, *Stability of Time-Delay Systems*, New York, NY, USA: Springer, 2003.

[19] F. Gouaisbaut and D. Peaucelle, "Delay-dependent robust stability of time delay systems," *IFAC Proceedings Volumes*, vol. 39, no. 9, pp. 453–458, Jul.2006.

[20] X. L. Zhu and G. H. Yang, "Jensen integral inequality approach to stability analysis of continuous-time systems with time-varying delay," *IET Control Theory & Applications*, vol. 2, no. 6, pp. 524–534, Jun. 2008.

[21] H. Y. Zhang, L. L. Xiong, Q. Miao, Y. M. Wang, and C. Peng, "A new integral inequality and delay-decomposition with uncertain parameter approach to the stability analysis of time-delay systems," *Journal of Difference Equations*, vol. 2016, pp. 6748170, Feb. 2016, doi: 10.1155/2016/6748170.

[22] S. Y. Xu, J. Lam, B. Y. Zhang, and Y. Zou, "New insight into delay-dependent stability of time-delay systems," *International Journal of Robust and Nonlinear Control*, vol. 25, no. 7, pp. 961–970, May 2015.

[23] H. Y. Shao, "New delay-dependent stability criteria for systems with interval delay," *Automatica*, vol. 45, no. 3, pp. 744–749, Mar. 2009.

[24] R. Tempo, G. Calafiore, and F. Dabbene, *Randomized Algorithms for Analysis and Control of Uncertain Systems with Applications*, 2nd ed., London: Springer-Verlag, 2013.

[25] Y. Ebihara, D. Peaucelle, and D. Arzelier, *S-Variable Approach to LMI-Based Robust Control*, London: Springer-Verlag, 2015, doi: 10.1007/978-1-4471-6606-1.

[26] H. M. Soliman and M. M. Sadek, "Resilient static output feedback power system stabiliser using PSO-LMI optimisation," *International Journal of Systems, Control and Communications*, vol. 5, no. 1, pp. 74–91, May 2013, doi: 10.1504/IJSCC.2013.054147.

[27] P. Kundur, *Power System Stability and Control*, Beijing: China Electric Power Press and McGraw Hill, 2001.

[28] S. Casoria. (2017, Sep.). Sequential AC-DC load flow method for two-terminal HVDC networks (Version 2), *Ac Generators*. [Online]. Available: https://cn.mathworks.com/matlabcentral/fileexchange/35929-sequential-ac-dc-load-flow-method-for-two-terminal-hvdc-networks-version-2-1-.

Wencheng Wu received the B.S. and M.S. degrees in Electrical Engineering from the Southwest Jiaotong University (SWJTU), Chengdu, in 2000 and 2003, respectively. He is currently pursuing a Ph.D. degree in Electrical Engineering from the SWJTU.

In 2003, he joined the Southwest Electric Power Design Institute. In 2009, he became a Licensed Electrical Engineer. He has participated in 7 HVDC/UHVDC projects' system studies, including the Yun-Guang, the first ±800 kV UHVDC project in the world. He has published more than 20 articles and holds five patents. His research interests include power system planning, operation, control, and engineering design.

Xiaoru Wang (M'02–SM'07) received a B.S. degree and an M.S. degree from Chongqing University, China, in 1983 and in 1988 respectively, and a Ph.D. degree from Southwest Jiaotong University, China, in 1998. Since 2002, she has been a Professor in the School of Electrical Engineering, Southwest Jiaotong University. Her research interests concentrate in the areas of power system operations, dynamics, protection and emergency controls.

Baorong Zhou received a B.S. degree from Wuhan University, Wuhan, China, in 1996, and M.Eng and Ph.D degrees from Tianjin University, Tianjin, China, in 2001 and 2005, respectively. From 2004 to 2010, he was a Power Planning Engineer with the China Southern Power Grid, Guangzhou, China. He is a Senior Power Expert with the Electric Power Research Institute since 2016. His current research interests include power system planning, and power system stability and control.

Hong Rao received a B.S. degree from the Huazhong University of Science and Technology, Wuhan, China, in 1983. He is currently the President of the Electric Power Research Institute, China Southern Power Grid, Guangzhou, China, where he is the Chair of the State Key Laboratory of HVDC Transmission Technology. He is the Project Manager of several milestone HVDC projects in HVDC technology. His research interests include the development and application of advanced HVDC technologies and the development of DC grids. Mr. Rao is a China Regular Member of CIGRE SC B4 and the General Secretary of the HVDC and Power Electronics Committee of CSEE. He was awarded the IEEE PES UNO LAMN HVDC Award in 2018.